Journal of Power Sources 194 (2009) 1099–1104

Contents lists available at ScienceDirect

Journal of Power Sources

journal homepage: www.elsevier.com/locate/jpowsour

Short communication

Electrochemical evaluation of rutile TiO_2 nanoparticles as negative electrode for Li-ion batteries

P. Kubiak[a], M. Pfanzelt[a], J. Geserick[b], U. Hörmann[c], N. Hüsing[b], U. Kaiser[c], M. Wohlfahrt-Mehrens[a,*]

[a] ZSW-Center for Solar Energy and Hydrogen Research, Helmholtzstrasse 8, D-89081 Ulm, Germany
[b] University of Ulm, Institute of Inorganic Chemistry I, Albert Einstein Allee 11, D-89081 Ulm, Germany
[c] University of Ulm, Electron Microscopy Group of Material Science, Albert Einstein Allee 11, D-89081 Ulm, Germany

ARTICLE INFO

Article history:
Received 21 April 2009
Received in revised form 22 May 2009
Accepted 2 June 2009
Available online 17 June 2009

Keywords:
TiO_2
Rutile
Anode material
Lithium ion battery

ABSTRACT

Nanosized rutile TiO_2 has been prepared by sol–gel chemistry from a glycerol-modified titanium precursor in the presence of an anionic surfactant. The sample has been characterized by X-ray diffraction, nitrogen sorption, scanning electron microscopy (SEM), high resolution transmission electron microscopy (HRTEM) and electrochemical tests. Nanosized rutile TiO_2 has been electrochemically investigated using two potential windows: 1.2–3 V and 1–3 V. It exhibits excellent high rates capabilities and good cycling stability.

1. Introduction

New types of batteries are urgently needed to meet the pressing demands of future key technologies. The development of hybrid electric vehicles (HEV) and electric vehicles (EV) strictly depends on the cost and availability of batteries with high energy, power densities, safety and long life [1–3]. These requirements are not met by existing batteries. New batteries having specific features such as flexible design, high power, safety as well as long cycle life have to be developed. These new batteries will have better volumetric energy, abuse tolerance and power rate for both charge and discharge. Reasonable cost will be achieved by using proven Li-ion technology and low cost raw materials.

Many problems are due to the use of graphite-based anodes exhibiting poor performances under particular operating conditions, i.e. low temperatures and high charge/discharge rates. Therefore there is an increasing interest in the development of alternative anode materials with enhanced kinetics and high rate capabilities. Anodic materials based on titanium oxides are promising candidates as alternative materials to carbonaceous anodes due to their advantages in terms of cheapness, safety and toxicity (even compared to other potential anodic materials). Among the TiO_2 polymorphs, anatase [4–7] and TiO_2(B) [8,9] are considered as the most efficient materials. The electrochemical performance of anatase TiO_2 strongly depends on the morphology of the material [10–14]. Moreover its performance can be enhanced by the addition of conductive phases [15–17].

Lithium insertion into bulk rutile is negligible at room temperature, but reversible Li insertion into rutile at 120 °C in lithium polymer cells has been reported [4,18]. Recently, it has been demonstrated that Li can be reversibly inserted into nanosized rutile [19–23]. Lithium insertion/extraction into/from rutile is highly anisotropic proceeding via fast diffusion along the *c*-axis channels while Li diffusion in the *ab* planes is very slow. The theoretically calculated diffusion coefficients for Li^+ diffusion along the *c*-axis and *ab* plane are 10^{-6} cm^2 s^{-1} and 10^{-14} cm^2 s^{-1}, respectively [24–26]. Thus, the control of the morphology of rutile nanoparticles appears as one of the key points for an efficient electrochemical behaviour.

Generally, rutile TiO_2 is obtained by thermal treatment of anatase TiO_2. The metastable anatase phase irreversibly transforms into rutile at temperature higher than 450 °C depending on particle size and/or presence of impurities [27,28]. The formation of rutile by annealing anatase particles leads to particle growth, which is unfavourable for lithium insertion. The rutile structure can also be synthesized at room temperature by precipitation in aqueous media [20,21,23], ionic liquids [29–31] or under hydrothermal conditions [32–34].

In this study, nanosized rutile TiO_2 was synthesized via a hydrolytic sol–gel route applying a glycerol-modified precursor in presence of an anionic surfactant. Typically in sol–gel processing simple, commercially available alkoxides are used as precursors,

* Corresponding author. Tel.: +49 731 9530 601; fax: +49 731 9530 666.
E-mail address: margret.wohlfahrt-mehrens@zsw-bw.de (M. Wohlfahrt-Mehrens).

0378-7753/$ – see front matter © 2009 Elsevier B.V. All rights reserved.
doi:10.1016/j.jpowsour.2009.06.021

however, diol/polyol-modified starting molecules, such as the glycerol-modified one, have some distinct advantages, especially with respect to processing in the presence of surfactants [35–37]. The conditions of synthesis resulted in oriented "nano-whisker"-shaped rutile particles. The obtained material shows excellent electrochemical performances in terms of capacity, cyclability, stability and reversibility, especially at high charge/discharge rates.

2. Experimental

2.1. Synthesis of nanosized rutile TiO_2

In a typical synthesis, 1.53 g (5.32 mmol) sodium dodecylsulfate (SDS, Merck) were dissolved in 250 mL diluted hydrochloric acid (pH 0). To this solution, 6.4 g GMT (bis(1,2,3 trihydroxypropyl)titanate, prepared from titanium tetraisopropoxide and glycerol) corresponding to 26.6 mmol Ti, were added and the suspension was subsequently ultrasonically treated at 60 °C for 2 h. After ageing at 60 °C overnight, the resulting powder was centrifuged, washed with water (3 times) and dried at 60 °C overnight. The sample was calcined at 400 °C for 4 h for complete surfactant removal.

2.2. Structural and morphological characterization

X-ray diffraction measurements were performed using Cu Kα radiation (λ = 0.154 nm) on a Siemens D5000. SEM images were collected on a LEO 1530 VP. Transmission electron microscopy (TEM) was performed on a Titan 80–300 kV. Nitrogen porosimetry measurements were performed on a Autosorb MP1 instrument (Quantachrome). The surface area was calculated according to Brunauer, Emmet and Teller (BET) in the p/p_0 range of 0.05–0.3 and the pore size distribution was determined according to Barrett, Joyner and Halenda (BJH) from the desorption branch of the isotherm.

2.3. Electrode preparation and electrochemical measurements

The electrodes have been manufactured by preparing a slurry with the following composition: TiO_2:Super P:PVDF = 76:12:12 wt.%. The slurry was coated on an aluminum foil as current collector using the "doctor blade" technique (thickness 150 μm) and dried at 40 °C/1 h. Circular electrodes were punched from the foil, pressed for better contact of the material and aluminium current collector and dried (130 °C) under vacuum

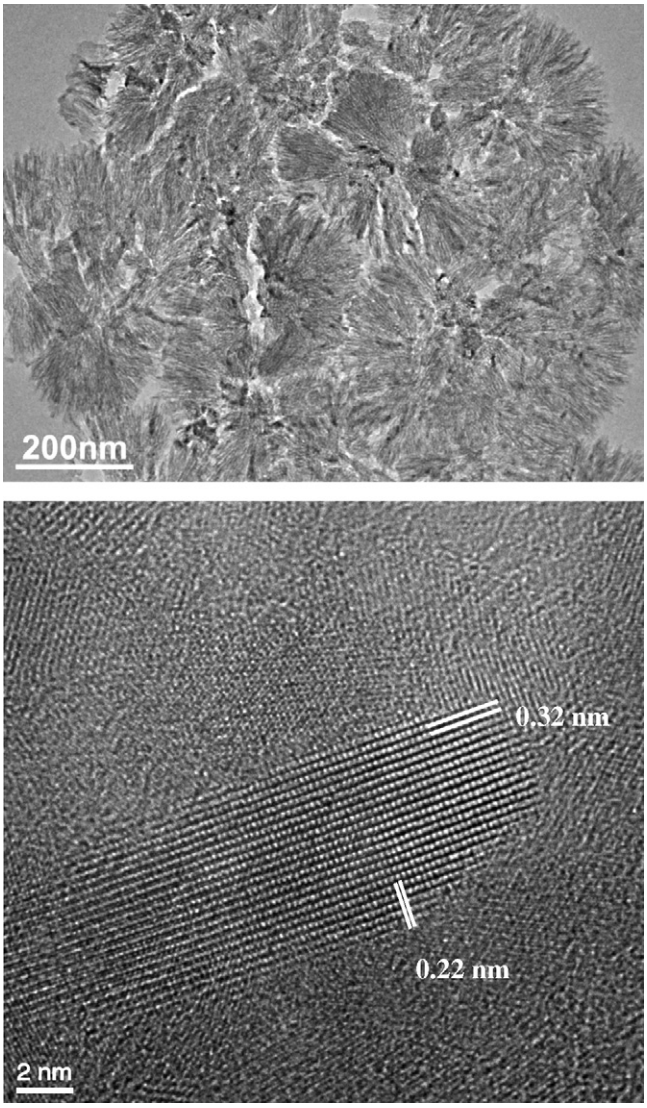

Fig. 2. TEM micrographs of nanosized rutile TiO_2.

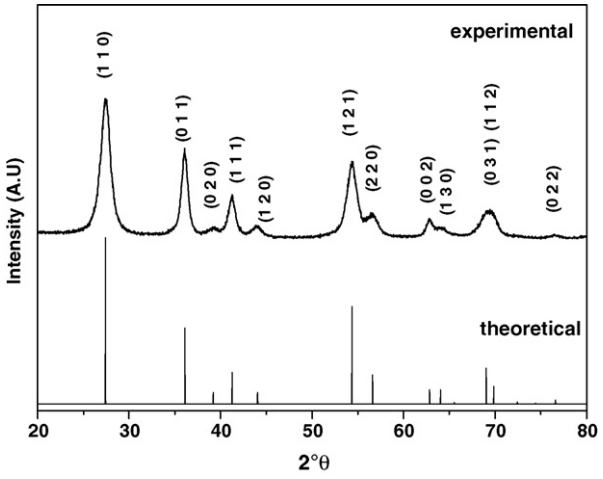

Fig. 1. X-rays diffractogram of nanosized rutile TiO_2 after calcination at 400 °C.

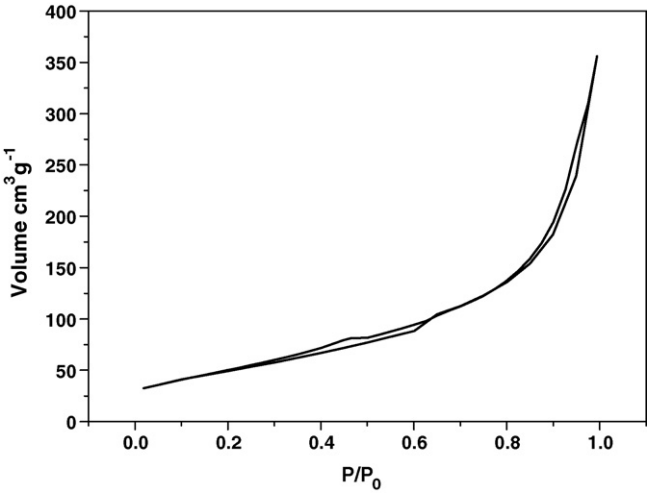

Fig. 3. SEM pictures of nanosized rutile TiO_2.

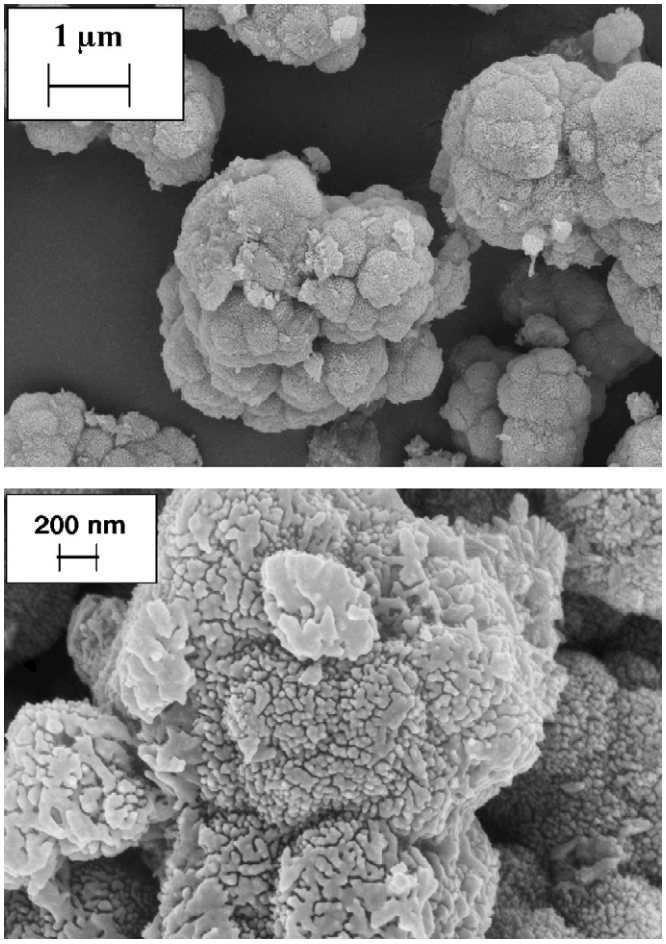

Fig. 4. SEM pictures of nanosized rutile TiO2.

overnight. The final electrodes have an active material loading of 2 mg cm^{-2}.

The electrochemical measurements were performed using three-electrode cells assembled in an argon glove box (MBRAUN). Metallic lithium was used as reference and counter electrodes, glass microfiber (Whatman, GF/A) as separator and 1 M $LiPF_6$ in EC:DMC (1:1 by wt.%) (UBE Industry, Japan) as electrolyte. The maximum x in Li_xTiO_2 is assumed to be 1 (335 mA h g^{-1}) and thus, the charging rates in these measurements were based on the following relationship: 1C = 0.335 A g^{-1}. All the measurements were carried out at room temperature using a VMP/Z (Princeton, Biologic) electrochemical workstation. All potentials are given vs. Li/Li$^+$.

3. Materials characterization

Generally, low temperature hydrolysis and condensation of titanium-based precursors leads to the formation of amorphous or anatase phases, sometimes even given nanoparticulate powders. Usually the thermodynamically stable rutile phase is prepared at the micro-scale range under severe conditions (high temperature or hydrothermal treatment). In this work nanoscale TiO_2 rutile has been synthesized via a hydrolytic sol–gel route from a glycerol-modified titanium precursor in presence of the anionic surfactant (SDS) at pH 0. The obtained solid was calcined at 400 °C/air for complete surfactant removal. Fig. 1 shows the XRD patterns after calcination. All the diffraction peaks can be indexed as rutile phase without the presence of other phases. The calculated cell parameters: a = 2.575 Å and c = 2.980 Å are in good agreement with the reference values (JCPDS 21-1276 a = 4.593 Å; c = 2.959 Å). The resulting sample was also investigated by HRTEM (Fig. 2). The rutile TiO_2 showed a significant growth anisotropy, i.e. the whiskers revealed a high aspect ratio with the diameter of the whiskers measuring approximately 4–5 nm and the length exceeding 40–50 nm even after calcination. The needles are aggregated to radial bunches, thus forming nanowhiskers arrays. In addition, a clear preferential orientation of the growth direction in [1 1 0] can be observed in the HRTEM images. The lattice distance of 0.32 nm corresponds to the (1 1 0) d-spacing. The lattice distance 0.22 nm corresponds to the (2 0 0) d-spacing. In addition, to the interesting morphology, the nanosized rutile TiO_2 exhibits a rather high specific surface area of 181 m^2 g^{-1}. The nitrogen ad- and desorption isotherms, in Fig. 3, can be classified as type III according the classification by Brunauer et al. [38], which is characteristic of a non-porous material. The SEM pictures are presented in Fig. 4. The nanosized rutile whiskers are agglomerated to cauliflower-like aggregates of several μm, thus favouring the contact between the active material and the electrolyte. In summary, the applied synthesis protocol offers a reproducible and versatile access to nanoscale rutile particles with a good control of the resulting physical properties (structure and morphology) of the material.

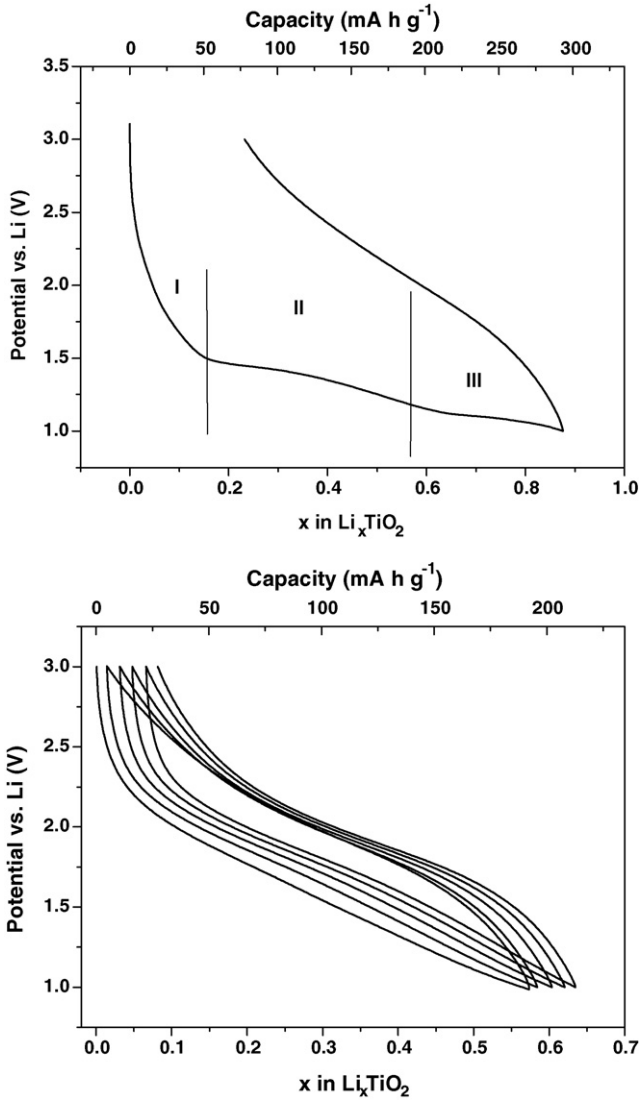

Fig. 5. Galvanostatic curves of TiO_2 rutile C/5 between 1 and 3 V vs. Li$^+$/Li. 1st cycle (top) 2nd–6th cycles (bottom).

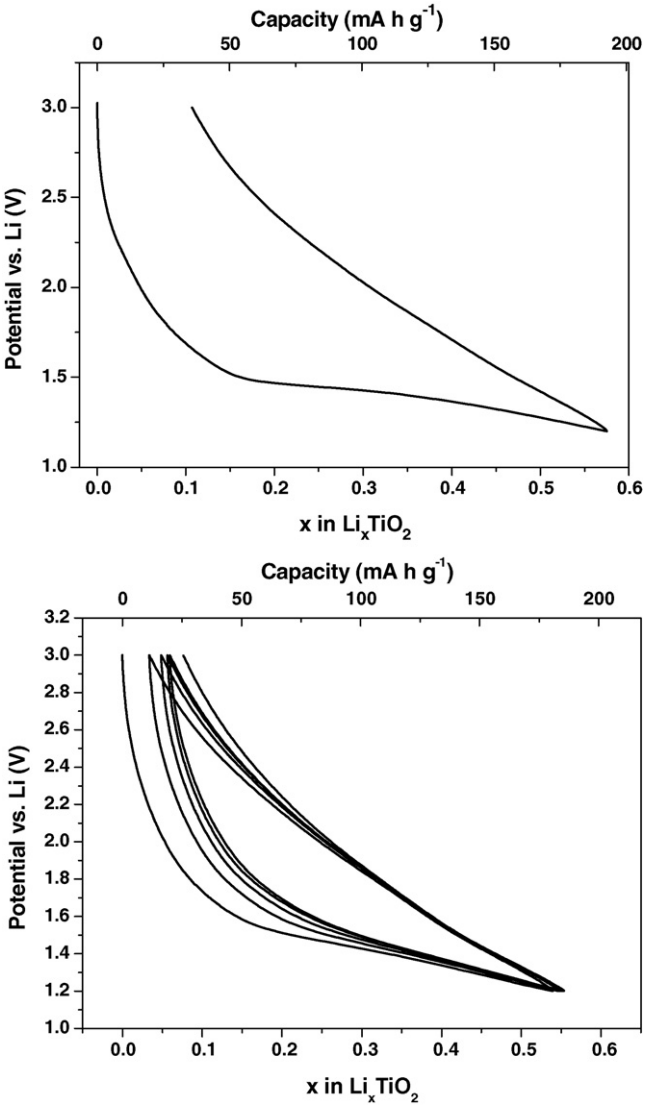

Fig. 6. Galvanostatic curves of TiO_2 rutile at C/5 between 1.2 and 3 V vs. Li^+/Li. 1st cycle (top) 2nd–6th cycles (bottom).

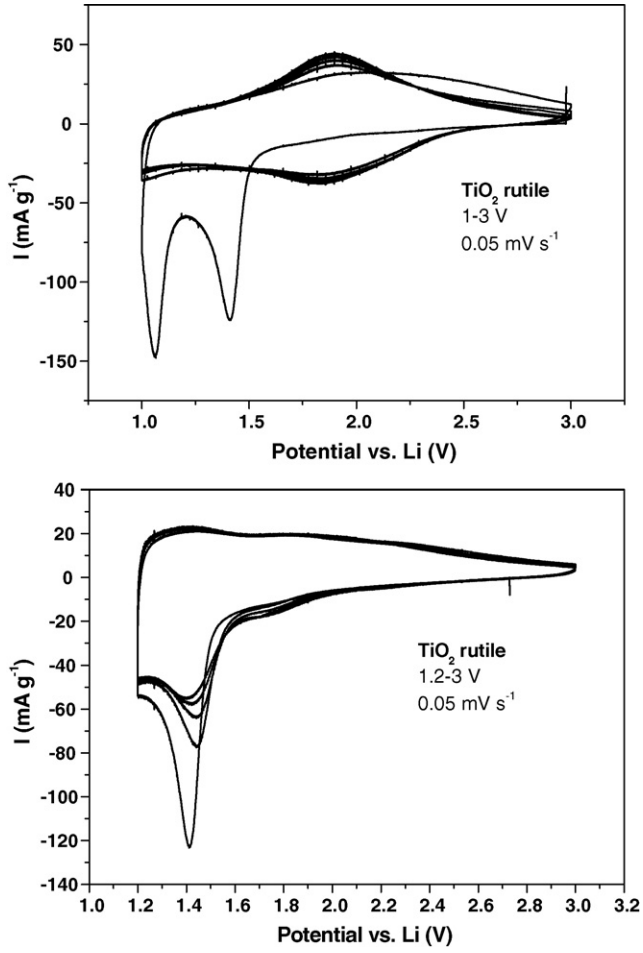

Fig. 7. Cyclic voltammetry for rutile TiO_2 in 1 M $LiPF_6$ EC/DMC (1/1, w/w), scan rate 0.05 mV s^{-1}, potential window 1–3 V (top) 1.2–3 V (bottom).

4. Electrochemical evaluation

The lithium insertion/extraction into TiO_2 rutile can be described by the following equation:

$$TiO_2 + x(Li^+ + e^-) = Li_xTiO_2$$

The galvanostatic discharge–charge curves at current density 33.5 mA g^{-1} (C/5) of nanosized rutile TiO_2 between 1 and 3 V vs. Li^+/Li is presented in Fig. 5. The first lithium insertion leads to a capacity of about 295 mA h g^{-1} corresponding to 0.88 Li per mol of TiO_2. Three distinct regions can be observed during the first discharge. The first step of Li insertion is an initial potential drop from OCV to about 1.4 V. The amount of inserted Li corresponds to 0.15 Li per mol of TiO_2. This phenomenon is commonly observed for nanometer sized materials. The amount of inserted lithium during this first potential drop strongly depends on the crystallite size and surface area of the material [10,39,40]. After the first initial potential drop a plateau can be observed at 1.4 V where 0.42 Li is inserted. The third part corresponds to a second plateau at 1.1 V. Important structural changes have been observed at 1 V by different groups. However, the exact structure of the obtained phase – hexagonal or cubic $LiTiO_2$ – is still under discussion. The identification of the structural modification after the first discharge is rather difficult due to the broadening of the X-rays diffraction peaks during Li insertion. Chemical lithiation by reaction of TiO_2 with *n*-butyllithium [41] or metal lithium by mechanical grinding [20] leads to the same controversial results. The profile voltage during the first charge is a smooth sloped curve ascribed to a solid solution domain reaction. No reversible plateaus can be observed suggesting that the first lithium insertion results in an irreversible phase transformation. A capacity loss of 60 mA h g^{-1} (0.18 Li) has been measured during the first cycle. The subsequent cycles showed sloped curves typical of lithium insertion/extraction in a solid solution domain. It can be seen that 0.57 Li can be inserted/extracted reversibly corresponding to a capacity of 190 mA h g^{-1}.

The same kind of experiment has been performed by limiting the discharge potential cut-off to 1.2 V. In these conditions, the first discharge is limited to the plateau at 1.4 V (Fig. 6). The limitation of the potential leads to a lower capacity (190 mA h g^{-1}) but also to a lower irreversible capacity loss (35 mA h g^{-1}). A reversible capacity of 168 mA h g^{-1} (0.5 Li) can be seen in the subsequent cycles. In both cases we can observe reversibility and high stability. The obtained curves differ from their shape suggesting that the Li insertion proceeds in different mechanisms depending on the potential window. After several cycles between 1.2 and 3 V the potential cut-off has been decreased to 1 V. The second plateau occurring at 1.1 V is then observed.

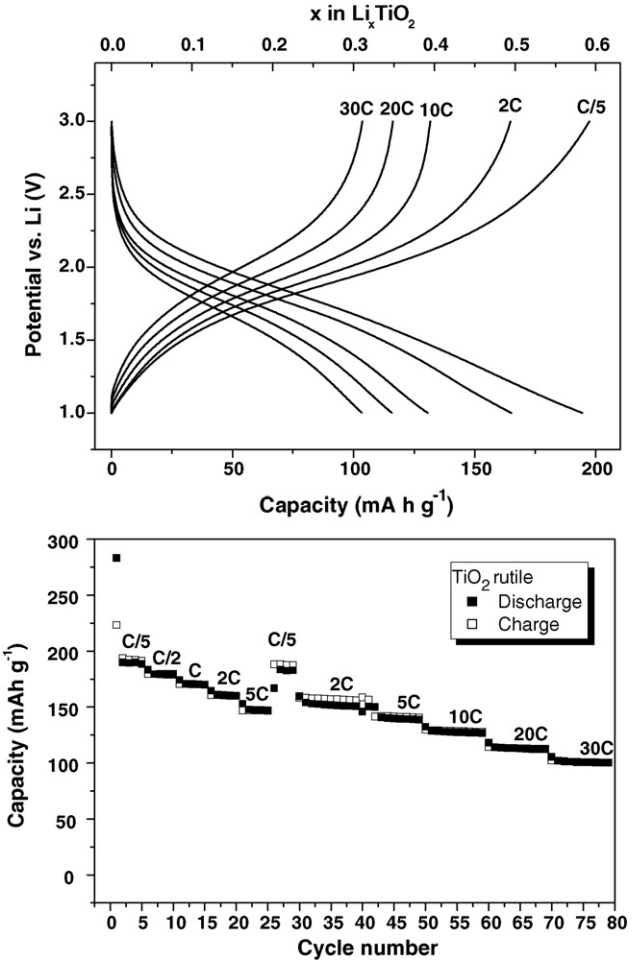

Fig. 8. Charging rates and capacity.

Cyclic voltammetry has been carried out between 1–3 V and 1.2–3 V on nanosized rutile at a scan rate of 0.05 mV s^{-1} for 5 cycles. The obtained voltammograms are presented in Fig. 7a and b. The first cycle between 1 and 3 V shows two cathodic peaks at 1.4 and 1.1 V. These peaks are ascribed to an irreversible phase transformation from TiO_2 to $LiTiO_2$. The subsequent cycles show reduction and oxidation peaks at about 1.8 V, which are consistent with lithium insertion/extraction in $LiTiO_2$ [20]. An increase of the intensity of these current peaks upon cycling can be observed indicating better kinetics.

By limiting the cut-off voltage to 1.2 V the cyclic voltammograms display the first reduction peak at 1.4 V and no distinct anodic peak (Fig. 6b). Usually, the presence of such a defined peak reveals a two-phases transition. In the subsequent cycles, this peak is still present with lower intensity. The recurrence of the peak indicates that the rutile structure is recovered during lithium extraction. The weaker intensity may indicate a decrease in the crystallite size (nano-crystallization). Wagemaker et al. claimed that the phase transformation from nanosized rutile TiO_2 to $LiTiO_2$ involves an intermediate phase $Li_{0.5}TiO_2$ (space group $P2/m$) with a "rutile-like" structure [41], which is consistent with our findings. The formation of $Li_{0.5}TiO_2$ is accompanied by a small volume increase and little atomic rearrangement. On the contrary the second phase transition involves a drastic atomic rearrangement and is not reversible. The different mechanisms for the phase transformation from TiO_2 to $LiTiO_2$ and the role of the different phases on their electrochemical behaviour are still a subject for further investigation.

Other important parameters for electrode materials are high rate capability and cycling stability. On Fig. 8 the voltage profile and the discharge/charge capacity evolution of nanometer-sized rutile TiO_2 at increasing current from C/5 to 30C are presented. The specific capacity shows excellent values for charging rates up to 30C. Indeed, the measured specific capacities are 190 mA h g^{-1} at a rate of C/5; decreasing to 179 mA h g^{-1} at C/2, 170 mA h g^{-1} at C, 151 mA h g^{-1} at 2C, 138 mA h g^{-1} at 5C, 127 mA h g^{-1} at 10C, 112 mA h g^{-1} at 20C, and finally, 100 mA h g^{-1} at 30C. In summary, rutile TiO_2 displays high capacities, excellent reversibility and stability upon cycling. This high rate capability is ascribed to shorter transport lengths for both electronic and Li^+ transport as well as a higher electrode–electrolyte contact area due to the high surface area.

5. Conclusion

The electrochemical lithium insertion into nanosized rutile TiO_2 synthesized using a glycerol-modified titanium-precursor and an anionic surfactant as a structure-directing agent has been investigated. It shows high charging/discharging capabilities and remarkable stability, which makes it a promising anode material for high-power lithium-ion batteries. These results are a further example of the advantages of nanostructured materials in the field of lithium-ion batteries.

Acknowledgements

Financial support from BMBF in the framework of the LISA project (03SF0327A) is gratefully acknowledged. J. Geserick and U. Hörmann acknowledge financial support by Deutsche Forschungsgemeinschaft (DFG) within the Priority Programme (SPP 1181).

References

[1] A.S. Aricó, P. Bruce, B. Scrosati, J.M. Tarascon, W. van Schalkwijk, Nat. Mater. 4 (2005) 366.
[2] P.G. Bruce, Solid State Ionics 179 (2008) 752.
[3] P.G. Bruce, Chem. Commun. 19 (1997) 1817.
[4] B. Zachau-Christiansen, K. West, T. Jacobsen, S. Atlung, Solid State Ionics 28–30 (1998) 1176.
[5] T. Ohzuku, T. Kodoma, T. Hirai, J. Power Sources 14 (1985) 61.
[6] S. Huang, L. Kavan, I. Exnar, M. Grätzel, J. Electrochem. Soc. 142 (1995) L142.
[7] L. Kavan, M. Grätzel, J. Rathousky, A. Zukal, J. Electrochem. Soc. 143 (1996) 394.
[8] G. Armstrong, R. Armstrong, J. Canales, R. Garcia, P. Bruce, Adv. Mater. 17 (2005) 862.
[9] G. Armstrong, R. Armstrong, P. Bruce, P. Reale, B. Scrosati, Adv. Mater. 18 (2006) 2597.
[10] G. Sudant, E. Baudrin, D. Larcher, J.-M. Tarascon, J. Mater. Chem. 15 (2005) 1263.
[11] C. Jiang, M. Wei, Z. Qi, T. Kudo, I. Honma, H. Zhou, J. Power Sources 166 (2007) 239.
[12] L. Kavan, J. Rathousky, M. Grätzel, V. Shklover, A. Zukal, J. Phys. Chem. B 104 (2000) 12012.
[13] D. Fatthakova, M. Wark, T. Brezesinski, B. Smarsly, J. Rathousky, Adv. Funct. Mater. 19 (2007) 2087.
[14] P. Kubiak, J. Geserick, N. Hüsing, M. Wohlfahrt-Mehrens, J. Power Sources 175 (2008) 510.
[15] Y.G. Guo, Y.S. Hu, W. Sigle, J. Maier, Adv. Mater. 19 (2007) 2087.
[16] I. Moriguchi, R. Hidaka, H. Yamada, T. Kudo, H. Murakami, N. Nakashima, Adv. Mater. 18 (2006) 69.
[17] M. Mancini, P. Kubiak, J. Geserick, R. Marassi, N. Hüsing, M. Wohlfahrt-Mehrens, J. Power Sources 189 (2008) 585.
[18] W.J. Macklin, R.J. Neat, Solid State Ionics 53 (1992) 694.
[19] Y.S. Hu, L. Kienle, Y.G. Guo, J. Maier, Adv. Mater. 18 (2006) 1421.
[20] E. Baudrin, S. Cassaignon, M. Koesch, J.P. Jolivet, L. Dupont, J.M. Tarascon, Electrochem. Commun. 9 (2007) 337.
[21] M.A. Reddy, M.S. Kishore, V. Pralong, V. Caignaert, U.V. Varadaraju, B. Raveau, Electrochem. Commun. 8 (2006) 1299.
[22] C.H. Jiang, I. Honna, T. Kudo, H.S. Zhou, Electrochem. Solid-State Lett. 10 (2007) A127.
[23] D. Wang, D. Choi, Z. Yang, V.V. Viswanathan, Z. Nie, C. Wang, Y. Song, J.G. Zhang, J. Liu, Chem. Mater. 20 (2008) 3435.
[24] F. Gligor, S.W. de Leeuw, Solid State Ionics 177 (2006) 2741.
[25] O.W. Johnson, Phys. Rev. 136 (1964) A284.
[26] M.V. Koudriachova, N.M. Harrison, S.W. de Leeuw, Phys. Rev. B 65 (2002) 235423.
[27] P. Arnal, R. Corriu, D. Leclercq, H. Mutin, A. Vioux, J. Mater. Chem. 6 (1996) 1925.

[28] H. Zhang, J.F. Banfield, J. Mater. Chem. 8 (1998) 2073.
[29] H. Kaper, F. Endres, I. Djerdj, M. Antonietti, B.N. Smarsly, J. Maier, Y.S. Hu, Small 3 (2007) 1753.
[30] N.Y. Yu, L.M. Gong, H.J. Song, Y. Liu, D.H. Yin, J. Solid State Chem. 180 (2007) 799.
[31] Y. Zhou, M. Antonietti, J. Am. Chem. Soc. 125 (2003) 14960.
[32] Q.H. Zhang, L. Gao, Langmuir 19 (2003) 967.
[33] C. Wang, Z.X. Deng, Y.D. Li, Inorg. Chem. 40 (2001) 5210.
[34] H. Cheng, J. Ma, Z. Zhao, L. Qi, Chem. Mater. 7 (1995) 663.
[35] S. Hartmann, D. Brandhuber, N. Hüsing, Acc. Chem. Res. 40 (2007) 885.
[36] X. Jiang, T. Herricks, Y. Xia, Adv. Mater. 15 (2003) 1206.
[37] M. Pal, J. Serrano, P. Santiago, U. Pal, J. Phys. Chem. C 111 (2007) 96.
[38] S. Brunauer, P. Emmett, E. Teller, J. Am. Chem. Soc. 60 (1938) 309.
[39] J. Jamnik, J. Maier, Phys. Chem. Chem. Phys. 5 (2003) 5215.
[40] J. Maier, Solid State Ionics 148 (2002) 367.
[41] W.J. Borghols, M. Wagemaker, U. Lafont, E. Kelder, F.M. Mulder, Chem. Mater. 20 (2008) 2949.